



Original article

Relationships between urbanization, tree morphology, and carbon density: An integration of remote sensing, allometric models, and field survey

Jian Lin ^{a,*}, Qin Ma ^b, Yang Ju ^c, Hongsheng Zhang ^d, Qiang Wang ^{e,f}, Bo Huang ^{g,h}^a Sierra Nevada Research Institute, University of California, Merced, Merced, CA 95340, USA^b School of Geography, Nanjing Normal University, Nanjing 210023, China^c School of Architecture and Urban Planning, Nanjing University, Nanjing 210093, China^d Department of Geography, The University of Hong Kong, Pokfulam, Hong Kong^e School of Geographical Sciences, Fujian Normal University, Fuzhou 350007, China^f State Key Laboratory for Subtropical Mountain Ecology of the Ministry of Science and Technology and Fujian Province, Fujian Normal University, Fuzhou 350007, China^g Department of Geography and Resource Management, The Chinese University of Hong Kong, Shatin, Hong Kong^h Institute of Space and Earth Information Science, The Chinese University of Hong Kong, Shatin, Hong Kong

ARTICLE INFO

ABSTRACT

Keywords:

Urban forestry

Natural climate solutions

Carbon distribution

Remote sensing

Urban trees store and sequester large amounts of carbon and are a vital component of natural climate solutions. Despite the well-recognized carbon benefits of urban trees, there is limited effort to examine how spatial distribution of carbon density varies across distinctive social, demographic, and built dimensions of urban landscapes. Moreover, it is unclear whether specific aspects of landscape structure and design could help increase carbon densities in urban trees. Here, we produced a fine-resolution carbon density map of urban trees in New York City (NYC) by integrating high-resolution land cover map, LiDAR-derived tree metrics, i-Tree Eco, and field survey data. We then explored spatial variations of carbon density across the gradients of urban development intensity, social deprivation index, and neighborhood age, and we examined the relationships between carbon density, and fragmentation, aggregation, size, and shape of tree canopy cover. We find that carbon stored in urban trees in NYC is estimated as 1078 Gg, with an average density of 13.8 Mg/ha. This large amount of carbon is unevenly distributed, with carbon densities being highest in Bronx and in open parks and street trees. Furthermore, carbon densities are negatively associated with urban development intensity and the social gradient of deprivation. Regarding the impacts of tree morphology on carbon density, our results show that while the amount of tree cover is the most influential factor in determining carbon density, small-sized forest patches and moderate levels of forest edges are also conducive to increasing carbon densities of urban trees. To incorporate urban forestry into developing innovative, effective, and equitable climate mitigation strategies, planners and decision makers need to identify the optimal spatial configuration of urban forests and invest in tree planting programs in marginalized communities.

1. Introduction

1.1. Urban forestry as a natural climate solution

Urbanization and global warming can result in many climate-change hazards that jeopardize the goal of building ecologically vital and socially just cities (Hobbie and Grimm, 2020). To alleviate these inevitable climate impacts, different sectors in urban systems have explored their ways to identify the total carbon mitigation potentials and alternative

low-carbon pathways. Great carbon mitigation potentials have been found in several sectors, such as energy systems, transport, buildings, and industry (Guan et al., 2018). Nevertheless, these efforts have not included the mitigation potential from urban forestry.

As a nature-based strategy, urban forestry sequesters and stores significant amounts of carbon in their soils and woody and foliar biomass (Pregitzer et al., 2021). Urban forests have been increasingly recognized as an essential carbon sink. There is growing evidence that the biological carbon stored in urban forests is substantially greater than

* Correspondence to: 5200 Lake Road, Merced, CA 95343, USA.

E-mail address: jlin270@ucmerced.edu (J. Lin).

previously assumed (Davies et al., 2013). For example, the total carbon storage in urban forests is estimated as 643 million tons in US (Nowak et al., 2013), 34,000 kt in Canada (Pasher et al., 2014), and 18.7 million tons in 35 major Chinese cities (Chen, 2015). In addition to the total amount, several empirical studies have shown that urban forests could serve as an effective carbon mitigation strategy in terms of carbon storage per unit area, quantified as carbon density. For example, the average carbon density for urban forests is 89 Mg/ha for Seattle, WA and 53.6 Mg/ha for Charlotte, NC, which is larger than or at a similar level as the average value of 53.5 Mg/ha for all US forests (Godwin et al., 2015; Hutyra et al., 2011). As the continuation of unprecedented urbanization and the expansion of urban areas in the coming decades, urban forests are expected to play a more critical role in offsetting carbon emissions and mitigating climate change, in addition to providing several co-benefits (e.g., residential energy conservation, air pollutant removal, and recreation opportunities) for urban sustainable development (Lin et al., 2019).

1.2. Mapping carbon density in urban trees

To incorporate urban forests into climate mitigation efforts and leverage more resources for tree management, it is critical to accurately quantify and map carbon stored in urban forests and characterize spatial heterogeneity of carbon density across the multi-dimensional urban landscape. Transfer functions are frequently employed to map carbon density in urban trees by relating remote sensing data with in-situ measured plot-level carbon estimates. Roughly speaking, plot-level carbon storage is estimated by applying species-specific allometric equations to field measured tree height and/or diameter at breast height (DBH). Then the plot-level carbon storage is overlaid with remote sensing data to develop empirical relationships. Last, the resulting empirical relationships are employed to transfer the data from the plot sites to any sites where no field data exist (McPherson et al., 2013; Raciti et al., 2014; Sun et al., 2019). We grouped the transfer function approach above into four categories based on different methods used in linking field measurements with remotely sensed datasets, i.e., Land Use/Land Cover (LULC), Tree Canopy Cover (TCC), Optical Imagery Derived-Vegetation Indices (VI), and Light Detection and Ranging

(LiDAR) approaches (Table 1). Both the LULC and the TCC approaches are based on carbon densities, namely they apply carbon density estimators per LULC type or TCC area to produce maps of carbon stocks in grid cells. The LULC-based approach is adopted by the InVEST Carbon Storage and Sequestration module (<https://naturalcapitalproject.stanford.edu/>), while the TCC-based approach is employed by the i-Tree Landscape (<https://landscape.itreetools.org/>). It is generally believed that TCC-based estimates are more accurate than LULC-based estimates because a single LULC class may contain vegetation with different TCC values (McPherson et al., 2013).

Two other approaches, VI- and LiDAR-based, are gaining popularity (Table 1). Normalized difference vegetation index (NDVI) is a typical vegetation index that has been widely used to predict vegetation biomass. NDVI represents the vigor and density of vegetation, and thus is highly correlated with vegetation biomass. NDVI derived from medium resolution satellite imagery (e.g., Landsat with 30 m resolution) is not fine enough to detect the heterogeneity in carbon density, particularly for urban forests where trees clustered along the streets in relatively thin strips and small patches. Therefore, fine spatial resolution images (e.g., QuickBird and Worldview-2) are increasingly employed to calculate NDVI (Sun et al., 2019). However, regardless of their spatial resolutions, optical imagery derived-vegetation indices are impacted by the saturation problem that underestimates biomass over dense forests. This is because passive optical sensors cannot penetrate through the dense canopy (Lu, 2006). As an active remote sensing technology, LiDAR emits the laser pulses that penetrate through forest canopy, and thus is able to provide accurate three-dimensional tree structural parameters that are highly correlated to tree biomass. The LiDAR-based approach adopted a variety of height- and crown-related metrics to develop the best-fitting transfer modeling to estimate carbon density (Godwin et al., 2015; Raciti et al., 2014). Although the four approaches are widely used, they are rarely compared to provide guidance for producing spatially detailed maps of carbon density, particularly in urban settings. Here, we compare the estimation accuracies between TCC-, VI- and LiDAR-based approaches, and map carbon stored in urban trees with the most accurate method.

Table 1
A summary of transfer function approaches to map carbon storage in urban trees.

Study site	Plot number	Sampling method	Remote sensing data	Transfer functions	Reference
Land use/land cover approach					
Leipzig, Germany	190 plots	Stratified random sampling	Orthophotos	CD* per land cover	Strohbach and Haase (2012)
Leicester, UK	190 plots	Random sampling	QuickBird and aerial imagery	CD per landcover-land ownership	Davies et al. (2011)
Tree canopy cover approach					
Shenyang, China	213 plots	Stratified random sampling	QuickBird	CD per tree canopy cover	Liu and Li (2012)
Los Angeles and Sacramento, US	370/300 plots	Random sampling	QuickBird and aerial imagery	CD per tree canopy cover	McPherson et al. (2013)
Optical Imagery Derived-Vegetation Indices approach					
Changchun, China	159 plots	Stratified random sampling	Landsat	Carbon = 101.63* $e^{(4.9201*NDVI)}$	Ren et al. (2019)
Beijing, China	326 plots	Random sampling	SPOT 6	CD = 1.3287* $e^{(6.5621*NDVI)}$	Sun et al. (2019)
Syracuse, NY, US	190 plots	Stratified random sampling	Landsat	Carbon = 107.2* $e^{(0.0194*NDVI)}$	Myeong et al. (2006)
LiDAR approach					
Santa Barbara, CA, US	89 plots	Random sampling	LiDAR	Carbon is a function of forest structural metrics	Alonzo et al. (2016)
Charlotte, NC, US	75 plots	Random sampling	LiDAR & Aerial photography	3 transfer equations in Table 6	Godwin et al. (2015)
Boston, MA, US	73 plots	Random sampling	LiDAR & QuickBird	Biomass = 2.1015*crown height+ 0.8455	Raciti et al. (2014)
Berlin, Germany Charlotte, NC, US	318 trees 70 plots	Random sampling Random sampling	LiDAR & QuickBird LiDAR & Aerial photography	CD = exp(-2.48 + 2.4835*ln(DBH))/2 8 transfer regression models in Table 4	Schreyer et al. (2014) Singh et al. (2015)

* CD: carbon density

1.3. Urbanization, tree morphology and carbon storage

Spatially explicit maps of carbon storage are often employed to reveal spatial variations and hotspots of urban tree carbon across the multi-dimensional urban landscape, which in turn, provides guidance for urban greenspace planning and local carbon mitigation strategies. For example, intra-city variations of carbon densities have been examined across urban development intensity (Sun et al., 2019), urban-rural gradient (Hutyra et al., 2011), land use classes (McPherson et al., 2013), residential land development pattern (Godwin et al., 2015), and a range of sociodemographic indicators (Raciti et al., 2014). These studies found that there exist large spatial variations of urban tree carbon due to factors such as regional context (e.g., climate and soil), tree characteristics (e.g., extent of greenspace, species composition, stand density, and age structure), and local site conditions (e.g., tree management practices, and neighborhood age) (Godwin et al., 2015; McPherson et al., 2013). The large variation of carbon storage has important implications for urban forest management. For example, in a mixed-age forest in Beijing, Sun et al. (2019) interpret spatial variability of carbon storage as an indicator for carbon sequestration potential (e.g., areas of low carbon densities could be converted to that of high densities), and the identified great carbon mitigation potential can be realized through careful landscape planning.

Nevertheless, the effects of urbanization on tree carbon storage go beyond the above-mentioned studies. Urban development isolates, fragments, and degrades greenspace, with modifications to habitat heterogeneity and connectivity (Alberti, 2005). It is commonly believed that forest fragmentation could cause carbon emissions from tropical forests, independent of and in addition to forest loss. This phenomenon is probably due to increased disturbance and tree mortality and decrease in ecosystem productivity along forest edges (Brinck et al., 2017). While the levels of fragmentation and heterogeneity in urban landscapes tend to be high, there are relatively few studies examining their impacts on carbon stored in urban trees. Related to this, other aspects of tree morphology (e.g., size, shape, aggregation, separation of tree canopy cover) also receive little attention. Given a fixed amount of greenspace, could compact greenspaces provide more carbon benefits than irregularly shaped greenspaces? Would a few large greenspaces be preferable over many small greenspaces? Are there any size thresholds for effective carbon storage? Addressing these questions provides ready-to-use guidance for urban forest management and local climate mitigation strategies.

1.4. Objectives

To examine relationships between urbanization, tree morphology, and carbon density in cities, we employ high-resolution optical images, LiDAR-derived tree metrics, and field survey data to produce a citywide carbon density map and perform analyses based on the map. We take New York City (NYC) as a case study, and our objectives are to (1) quantify and map carbon stored in urban trees by comparing TCC-, VI- and LiDAR-based approaches; (2) explore spatial variability of carbon density across distinctive social, demographic, and built-environment dimensions of urban landscape; and (3) examine the relationships between carbon density and landscape metrics representing fragmentation, aggregation, size, and shape of tree canopy cover. These research efforts could reveal carbon mitigation potential of urban trees in NYC and help design local climate mitigation strategies. The findings could also aid in urban greenspace planning and urban forest management.

2. Methods

2.1. Study site

Our analysis focused on NYC, located in the northeastern United States. NYC is committed to achieving carbon neutrality by 2050

through 80 % greenhouse gas emissions reductions referencing to the 2005 baseline (NYC MOS, 2021). NYC is composed of boroughs of Brooklyn, Queens, Manhattan, The Bronx, and Staten Island (Fig. 1a), and the city occupies a land area of 778.2 km². NYC has a humid subtropical climate, with annual average temperature of 11.9 °C and annual precipitation of 1139 mm. As of 2020, there are around 5.2 million trees and 168 different tree species in NYC, which cover a 24 % land area (NYC Tree Facts, 2020). In 2007, NYC launched the ambitious Million-TreesNYC initiative (<https://www.milliontreesnyc.org/>) that aims to plant and care for one million new trees anywhere (e.g., urban parks, neighborhood streets, residential backyards, and schoolyards) across the city's five boroughs within 10 years. This planting campaign and many subsequent tree stewardship activities have significantly improved tree health and ensured the provision of desired ecosystem services, including carbon mitigation.

2.2. Field survey and i-tree eco

Field survey was conducted in summer 2013 by a field crew of two people. Field data were sampled and measured based on the i-Tree Eco protocols developed by the USDA Forest Service (i-Tree Eco Field Guide, 2021). Specifically, circular 0.1-acre plots were established citywide using simple random sampling (Fig. 1a), and within each plot, the attributes of all encountered woody species with a minimum DBH of 2.54 cm were measured. In total, there were 139 species and 1075 trees across 296 plots measured over NYC. The DBH of trees ranged from 2.5 to 121.7 cm (Fig. 1b), tree height ranged from 1.2 to 30.5 m (Fig. 1c), and the tree numbers in individual plots ranged from 0 to 71.

We applied field collected tree attributes (e.g., species, DBH, tree height) to i-Tree Eco (<https://www.itreetools.org/tools/i-tree-eco>), and the model calculated urban tree carbon storage for each individual tree. i-Tree Eco has a database of species-specific allometric equations (Nowak et al., 2013), and the equations can be summarized in the following four forms:

$$\text{Biomass} = \exp(\beta_1 + \beta_2 * \ln(DBH) + \frac{\sigma^2}{2}) \quad (1)$$

$$\text{Biomass} = \exp(\beta_1 + \beta_2 * \ln(DBH^2 * \text{HEIGHT}) + \frac{\sigma^2}{2}) \quad (2)$$

$$\text{Biomass} = \beta_1 * (DBH^{\beta_2}) \quad (3)$$

$$\text{Biomass} = \beta_1 * ((DBH^2 * \text{HEIGHT})^{\beta_2}) \quad (4)$$

where β_1 and β_2 are species-specific coefficients, DBH is measured at 1.37-m above the ground, HEIGHT is the total tree height (height from the ground to the top of the tree), and σ^2 is the variance of model errors, which is applied to correct the transformation bias when back-transforming predictions from logarithmic scale to original scale (Nowak, 1996). The choices of coefficient values (e.g., β_1 and β_2) and equation forms (e.g., Eq. 1–4) depend on the species matching process. For non-matching species, the average result from equations of the same genus is used (Nowak et al., 2008). The estimated whole tree biomass (including above- and below-ground biomass) was multiplied by a factor of 0.5 to convert to carbon storage (Nowak and Crane, 2002). By applying the above allometric equations to all the trees in plots, the mean carbon density per plot was calculated as 11.98 Mg/ha, with the values ranging from 0 to 133.37 Mg/ha; its standard deviation is 25.0 Mg/ha.

2.3. Mapping carbon storage and accuracy assessment

2.3.1. Remote sensing datasets

The tree canopy cover (TCC) data was derived from a fine-resolution land cover dataset provided via NYC OpenData (<https://opendata.cityofnewyork.us/>).

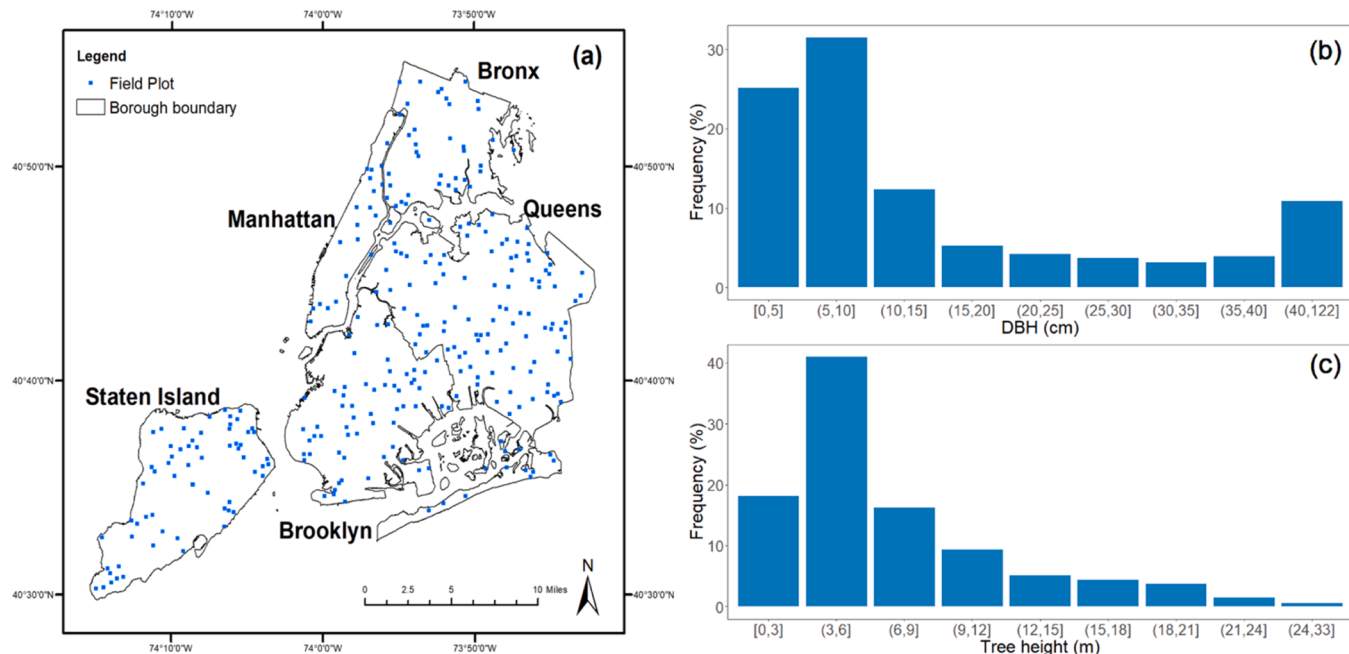


Fig. 1. Spatial distribution of field survey plot (a), and frequency distribution of tree DBH (b) and tree height (c).

cityofnewyork.us/). This land cover dataset was derived from a 2010 LiDAR survey and the 2009 4-band fine-resolution National Agriculture Imagery Program (NAIP) aerial imageries using object-based image analysis (O’Neil-Dunne et al., 2014). There were seven land cover classes mapped at 3-feet (about 0.9-meter) resolution, including (1) tree canopy, (2) grass/shrub, (3) bare earth, (4) water, (5) buildings, (6) roads, and (7) other paved surfaces. We generated TCC by setting the tree canopy class as 1 and non-tree class as no-data and resampling the data into 1-meter resolution to match with NAIP and LiDAR datasets (Fig. 2a). The TCC data were used as a mask for NAIP and LiDAR datasets to exclude non-tree areas.

We employed all available 1-meter resolution NAIP images in the Google Earth Engine from June to August 2013 to calculate NDVI. A total of 63 scenes were mosaiced together to cover the entire NYC, from

which NDVI was calculated (Fig. 2b). We overlaid the resulting NDVI map with TCC to mask out non-tree NDVI, from which we obtained the tree-NDVI map.

The LiDAR data were collected using a Leica ALS70 LiDAR system onboard a Cessna aircraft in two flight missions. The first mission was flown on August 5, 2013 at a nominal pulse spacing of 0.91 m, at 2286 m above ground level with an average side lap of 30 %. The second mission was flown between March and April, 2014 at 0.7 m nominal pulse spacing, 2286 m above ground level with an average side lap of 25 %. The LiDAR scan was performed at 9.25 cm root mean square error accuracy supported by ground control survey.

We generated a Canopy Height Model (CHM) by rasterizing the LiDAR point cloud at 1-meter resolution to match with TCC and NAIP-derived NDVI maps. The CHM was derived from the difference

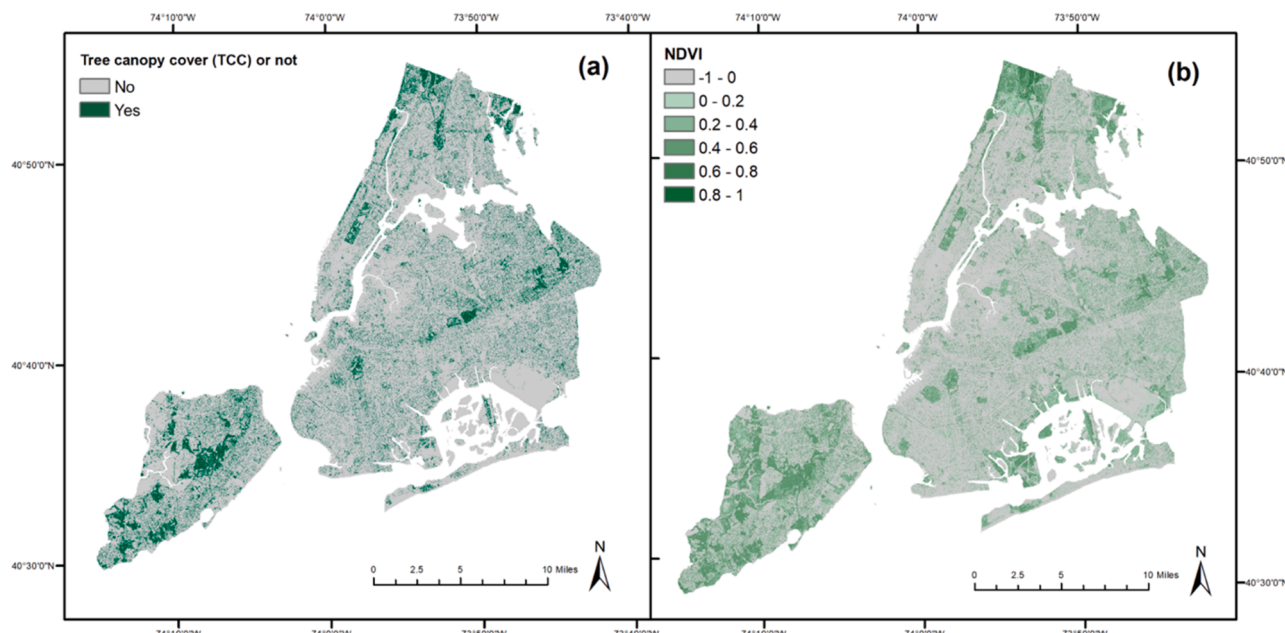


Fig. 2. Spatial distributions of tree canopy cover (a), and Normalized difference vegetation index (NDVI) (b) in NYC.

between Digital Surface Model and Digital Terrain Model generated from LiDAR point clouds using the Kriging Interpolation method (Guo et al., 2010) using LiDAR360 software (GreenValley International). The CHM was overlaid with TCC to mask out non-tree areas. We then overlaid tree-only CHM with field plot to generate LiDAR metrics for carbon density modeling. Three sets of LiDAR metrics were derived within each field plot, including the mean and max value of CHM (CHM mean and CHM max) and Canopy Cover calculated as the percentage of areas covered by canopy with a height over 2 m (Ma et al., 2017). The NDVI and LiDAR-derived metrics were all based on remote sensing data in 2013 or 2014, which match the field survey data. For TCC, it is based on land cover data in 2010 and we assumed that the growth of tree biomass during the 3-year period was negligible when compared to the existing tree biomass.

2.3.2. Carbon density model fitting

Based on the literature review (Table 1), we fitted and compared the carbon density models by employing the Tree Canopy Cover (TCC), Optical Imagery Derived-Vegetation Indices (VI), and Light Detection and Ranging (LiDAR) approaches, respectively. We considered CHM mean and CHM max as explanatory variables in the LiDAR approach. As for the model form, the linear form was adopted by the TCC and LiDAR approaches, the exponential form was used by the VI and LiDAR approaches (Table 1), and the quadratic form was also frequently employed by allometric equations. Therefore, we tested and compared the linear, quadratic, and exponential forms for all the TCC, VI, and LiDAR approaches.

We treated plot-level whole tree carbon (calculated by applying field measured DBH and tree height to species-specific allometric equations) as the ground truth. We assessed model accuracy by using a 10-fold cross-validation, where the field plots were first portioned into 10 equal-sized subsets with 9 subsets used for training and the remaining 1 subset used for validation. This cross-validation process was then repeated 10 times with each subset used exactly once for the validation. The coefficient of determination (R^2) and Root Mean Squared Error (RMSE) between estimated and measured carbon density were used to assess the model accuracy. Based on Chicco et al. (2021), the R^2 and RMSE were estimated as

$$R^2 = 1 - \frac{\sum_{i=1}^n (y_i - \hat{y}_i)^2}{\sum_{i=1}^n (y_i - \bar{y})^2} \quad (5)$$

$$RMSE = \sqrt{1/n \sum_{i=1}^n (y_i - \hat{y}_i)^2} \quad (6)$$

where y_i and \hat{y}_i is the observation and predicted value of a variable at point i, respectively; \bar{y} is the mean of a variable; and n is the number of observations. Based on the model accuracy assessment, we chose the optimal model to map the carbon density citywide. Since our ground truth measured the whole tree carbon, our developed carbon density model was also for the entire tree.

2.4. Variability of carbon density across urban landscapes

Based on the urban tree carbon storage map, we examined the variability of carbon density across multi-dimensional urban landscapes. Specifically, we compared the differences in carbon storage and carbon density across the administrative divisions of five boroughs (e.g., Brooklyn, Queens, Manhattan, Bronx, and Staten Island), and eight land use classes (e.g., one-two family residential, multi-family residential, residential-commercial mixed, commercial, industrial, open space, street, and public facilities & institutions). Land use classes were derived from the Parcel Land Use and Tax Ownership (PLUTO) map, which contained detailed land use codes for individual land parcels. For the

land use of streets, we employed NYC Planimetric Database to merge roadbeds, (e.g., traffic islands, curb edging, and medians with white paved markings), and sidewalks adjacent to roadbeds to create street polygons (Lin et al., 2021).

In addition, we also examined the variability of carbon density across the gradients of urban development intensity (UDI), neighborhood age, and socioeconomic status. Represented as the urbanization level, UDI was quantified by the percentages of impervious surface cover based on the high-resolution land cover map in NYC in 2010 (Sun et al., 2019). Neighborhood age was determined by the “Built Year” attribute of land use parcels from the PLUTO data, from which the median age of all constructed buildings on land parcels within a census tract was obtained to represent neighborhood age (McPherson et al., 2013). Rather than examining carbon density across individual socioeconomic measures, we employed a composite indicator, namely the social deprivation index (SDI) that aggregates multiple socioeconomic and demographic measures of deprivation to quantify and rank neighborhood disadvantage (Butler et al., 2013). SDI was created by applying the factor analysis to seven variables from the 2011–2015 5-year American Community Survey (ACS), and the seven variables included capture the social dimensions of income, education, employment, living status, housing quality, and transportation. The resulting SDI was normalized to a score between 0 and 100, with higher numbers suggesting a higher deprivation (Liaw et al., 2018). All the analyses were conducted by overlaying the urban tree carbon density map with the dataset of corresponding landscape dimensions in ESRI ArcGIS 10.8, and the carbon density and landscape information were then summarized at the census tract level to perform statistical analyses using R software (version 4.1.1) (R Core Team, 2022).

2.5. Relationships between tree morphology and carbon density

A variety of landscape metrics have been proposed to measure the composition and configuration of landscape patterns (Li and Wu, 2004). Considering the redundancy among metrics and their implications for urban greenspace planning, we selected six representative measures that indicate the abundance, fragmentation, aggregation, area size, and shape of tree canopy cover (Table 2). The metrics were calculated for census tracts based on 1-meter resolution tree canopy map in NYC using R packages “landscapemetrics”. The patch neighbors were defined by the “8-cell rule”.

We applied the random forest (RF) regression to explore the relationships between landscape metrics of TCC and carbon density. RF has ready-to-use measurements to quantify the relative importance of different landscape metrics. Specifically, when a landscape metric was excluded from the RF regression model, the mean decrease in prediction accuracy (indicated as the changes in MSE) within out-of-bag samples represents the relative importance of the corresponding variable in

Table 2
A description of landscape metrics employed in this study (McGarigal, 2002).

Metrics	Abbreviation (unit)	Description
Percent of tree canopy cover (TCC)	PTCC (%)	Proportional abundance of TCC in the landscape
Mean patch area	AREA_MN (ha)	Total patch area divided by patch number
Edge density	ED (m/ha)	The total perimeter of TCC patches per hectare
Largest patch index	LPI (%)	The proportion of the largest TCC patch within a census tract
Mean Euclidian nearest-neighbor distance	ENN_MN (m)	Mean distance to the nearest neighboring patch of TCC based on the edge-to-edge distance
Mean patch shape index	SHAPE_MN (unitless)	The average shape index of TCC patches within a census tract

predicating the variation of carbon density (Breiman, 2001). In addition, based on the RF regression model, partial dependence plots (PDPs) can be derived to examine the non-linear relationship between each variable and carbon density. PDP is a graphical description of the marginal effect of carbon density due to each variable by fixing all other explanatory variables at their mean values (Hastie et al., 2009). The RF model was trained using a 10-fold cross validation.

3. Results

3.1. Mapping carbon storage and accuracy assessment

Our model fitting results were displayed in Fig. 3. Based on the measurements of R^2 and RMSE derived from the cross-validation analyses (Fig. 4), we concluded that the CHMmean linear regression achieved the highest accuracy.

The CHMmean linear regression model was applied to the entire study area with tree canopy cover (Fig. 5). The results showed the total carbon storage in NYC is 1078 Gg (1 Gg = 10^9 g). The mean carbon density of 13.8 Mg/ha varying from 0 to 410.1 Mg/ha, with a standard deviation of 38.8 Mg/ha over the entire study area.

3.2. Variability of carbon storage across urban landscapes

Carbon stored in urban trees varied greatly across five boroughs and eight land use classes (Fig. 6). The carbon storage was the largest in Queens and Bronx, followed by Staten Island and Brooklyn, and Manhattan had the least amount of carbon (Fig. 6a). Queens had the largest amount of carbon due to a larger area of tree canopy cover, while Bronx was due to the largest carbon density. The carbon density in Bronx was

estimated as 18.3 Mg/ha, which was greatly larger than the other four boroughs (between 9.9 and 11.6 Mg/ha) (Fig. 6c). Regarding the land use classes, the ranking of carbon storage amount was open space & park lands > 1–2 family residential > street > multi-family residential > public facilities & institutions > residential-commercial mixed > commercial > industrial land (Fig. 6b). The carbon density across land use classes followed a similar pattern as carbon storage, except that street trees (12.2 Mg/ha) had a higher density than trees in 1–2 family residential land (10.0 Mg/ha). The carbon density differences varied greatly from 2.2 Mg/ha for industrial land to 26.1 Mg/ha for open space & park. The open space & park was the only land use that had a value above the city average (13.8 Mg/ha).

When examining across built and socio-demographic dimensions of urban landscape, the variations of carbon density in urban trees followed specific patterns (Fig. 7). In general, carbon density declined with the increases in impervious surface cover and SDI, but the declined rate was higher along the gradient of impervious surface than the gradient of SDI. This is probably due to that there was more variation of carbon density across the SDI dimension. In contrast, the relationship between carbon density and neighborhood age, indicated by the median year of constructed buildings in a census tract, was more complicated than a monotonically decreasing pattern. The carbon density declined over time until 1920, and the relationship roughly followed an inverted-U relationship that carbon density increased with neighborhood age to about the year 1950 and then declined over time.

3.3. Relationships between tree morphology and carbon density

The six landscape metrics jointly explained 91 % of the total variance in carbon density. PTCC was the most influential variable in determining

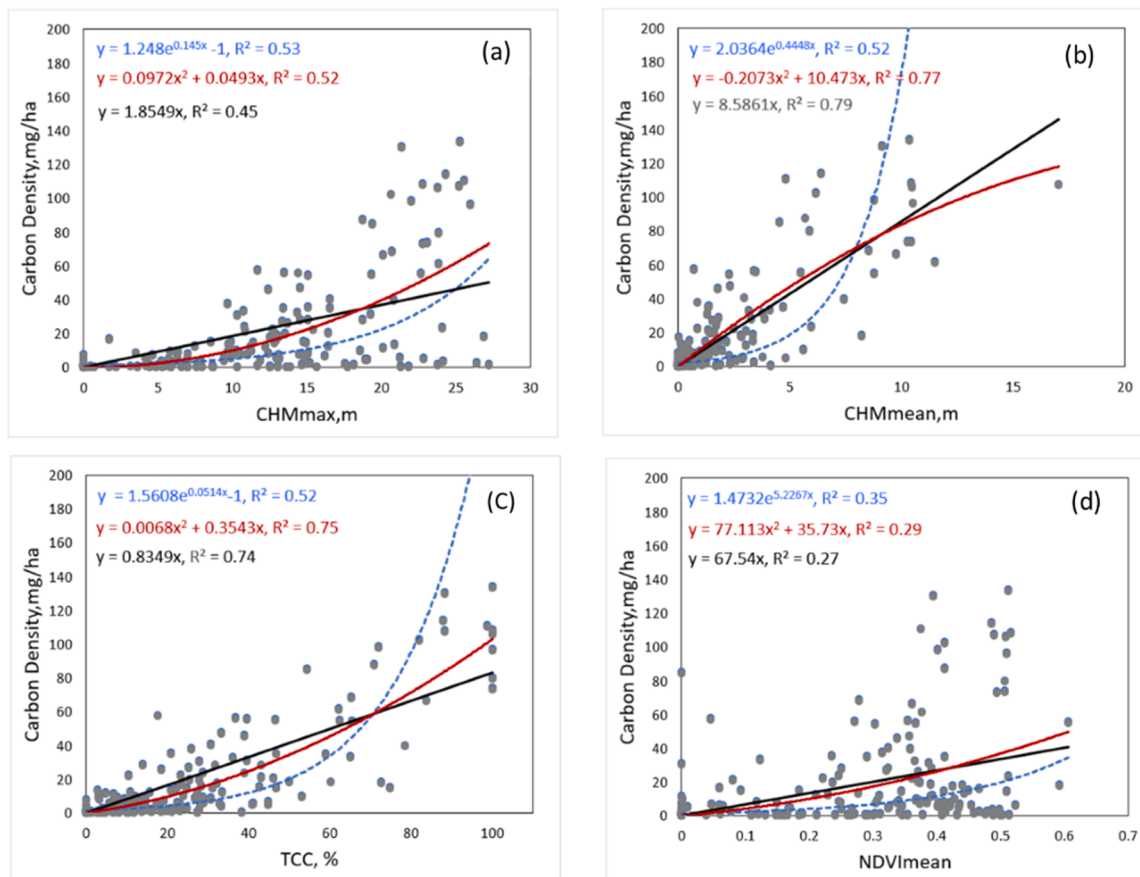


Fig. 3. Carbon density regression functions fitted from LiDAR derived CHMmax (a), CHMmean (b), TCC (c), and NAIP imagery derived NDVImean (d), using linear (black), quadratic (red), and exponential (blue) functions, respectively.

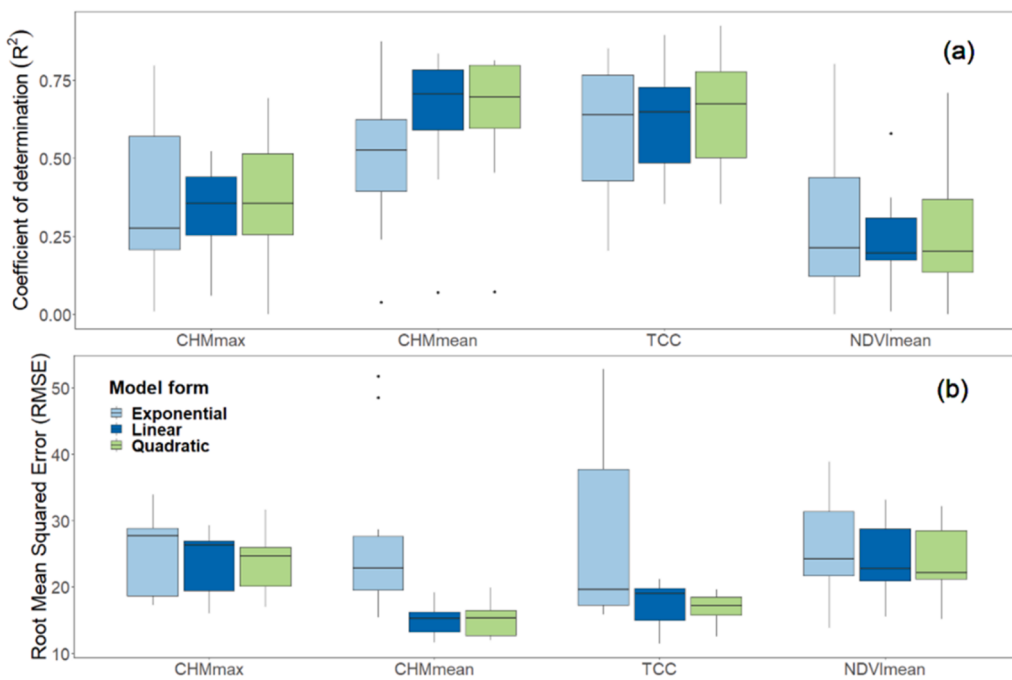


Fig. 4. The accuracy assessment based on a 10-fold cross-validation: (a) the coefficient of determination (R^2) and (b) the Root Mean Squared Error (RMSE). The total dataset was split into 10 equal-sized subsets, with 9 subsets used for training and the 1 subset used for validation. We repeated the process 10 times with each subset used exactly once for the validation.

carbon density (Fig. 8). For the other five metrics of spatial configuration, AREA_MN had the largest impact, ED and LPI had the moderate effects, while ENN_MN and SHAPE_MN had much smaller effects. The partial dependence analysis further revealed the detailed response of carbon density to individual metrics when holding all the other variables at their mean values. In general, the response curves can be grouped into two categories: nonlinear increases (PTCC, AREA_MN, ED, and LPI) and nonlinear decreases (ENN_MN and SHAPE_MN) (Fig. 9). In general, the more PTCC, the better. For AREA_MN, ED, and LPI, carbon densities increased to certain levels and then leveled off. For ENN_MN and SHAPE_MN, smaller values (indicating aggregated tree canopy patterns and compact shape of canopy cover) were associated with higher carbon densities.

4. Discussion

4.1. Comparing among different transfer functions

Among all the transfer function approaches, we found that the CHMmean (linear form) and TCC (linear form) approaches have achieved the highest accuracy (Fig. 4). This is consistent with McPherson et al. (2013) who apply the linear TCC approach to map carbon density in California, and Raciti et al. (2014) who find that biomass is a linear function of canopy height in Boston, MA. Although more complicated model forms (e.g., quadratic) may achieve satisfactory results, they may have the issue of overfitting and it is challenging to generalize to other geographic contexts. Surprisingly, our result concluded that the accuracy for the NDVI (exponential form) approach was relatively low, although this approach was frequently employed by previous studies (Table 1). In a recent study in Shanghai, China, Shen et al. (2020) also report that the accuracy (R^2) is unsatisfied when employing NDVI to estimate and map AGB. For the robust analyses, we replaced NDVI with EVI in the VI approach; in addition, we also incorporated several metrics (e.g., TCC, NDVI, LiDAR metrics) to develop multivariate regression models and random forest models. However, we achieved no better results than the CHMmean and TCC approaches (Therefore, the results were not displayed here). By considering model accuracy and

parsimony, as well as the data availability, we recommend the TCC and LiDAR approaches to develop transfer functions.

4.2. Carbon stored in urban trees and its spatial variability

Carbon stored in urban trees is often understudied (Sun et al., 2019), and their values in forest carbon accounting and regional inventories of carbon balance are largely ignored (Tang et al., 2016). This is probably due to small sizes of urban land areas and large amounts of greenhouse gas emissions from urban tree management (McPherson et al., 2013). Our results suggest that urban trees in NYC could store a large amount of carbon (1078 Gg), and the number is likely to be conservative as we didn't consider other natural carbon pools (e.g., litter and duff, soil, and groundcover) (Pregitzer et al., 2021). In addition, the carbon storage potential of urban trees in the future is large, considering that 18.0 % of the City's land is currently vegetated with shrubs and grassland that can be converted to forests with low cost and 24.6 % of land is asphalt or concrete surfaces (excluding roads and buildings) that are theoretically available but may not be feasible to convert into forests (Grove et al., 2014). Given this large potential, NYC aims to increase its tree canopy cover to 30 % by 2035 (Leff, 2016). The forestry sector is demonstrated to be a cost-effective way to combat climate change, as much of its mitigation opportunity can be achieved below current carbon market prices (Fargione et al., 2018). However, the current studies that examine the pathways to NYC's 2050 carbon neutrality goal do not emphasize the opportunity from urban forestry (NYC MOS, 2021). It is important to examine current capability and future potential of carbon uptake in the City's forestry and integrate it into the City's carbon neutrality pathways.

The large amount of carbon stored in urban trees varies greatly across landscapes. Carbon density in Bronx (18.3 Mg/ha) is much larger than the other four boroughs (between 9.9 and 11.6 Mg/ha), probably because Bronx occupies a relatively low level of impervious surface and is home to several large open parks and natural areas (e.g., Pelham Bay Park, Van Cortlandt Park, Bronx Park, and Ferry Point Park), which provide intact habitats and less disturbed conditions for tree growth. Regarding land uses, carbon densities are highest in open space and

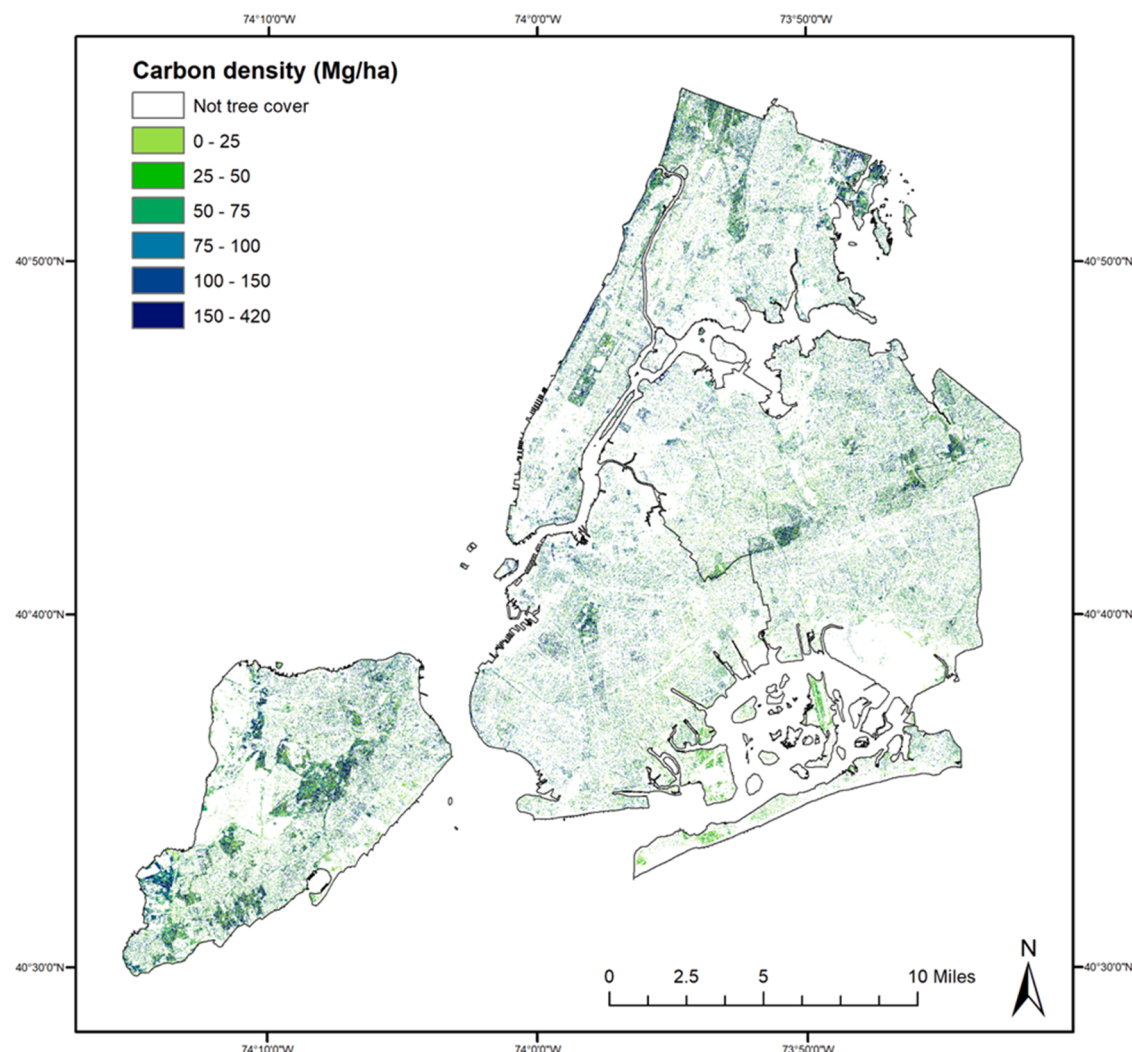


Fig. 5. Spatial distribution of above- and below-ground carbon stored in urban trees across New York City.

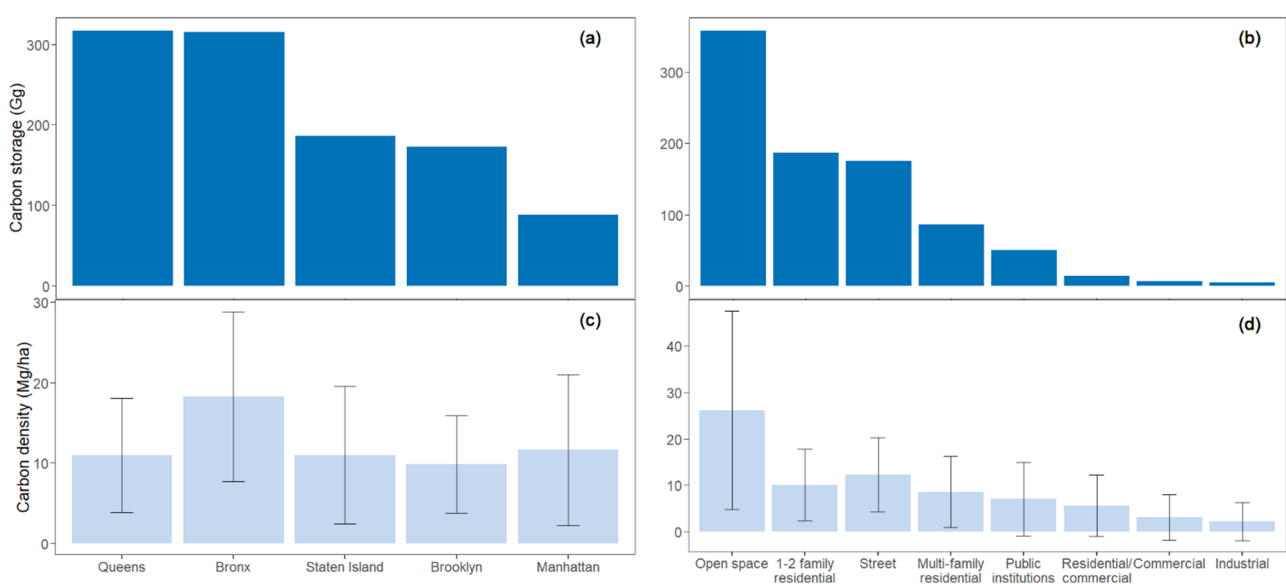


Fig. 6. Spatial variations of carbon in urban trees: carbon storage across five boroughs (a) and eight land uses (b), and carbon density across five boroughs (c) and eight land uses (d). The error bars in (c) and (d) represent \pm standard deviation of carbon density estimates.

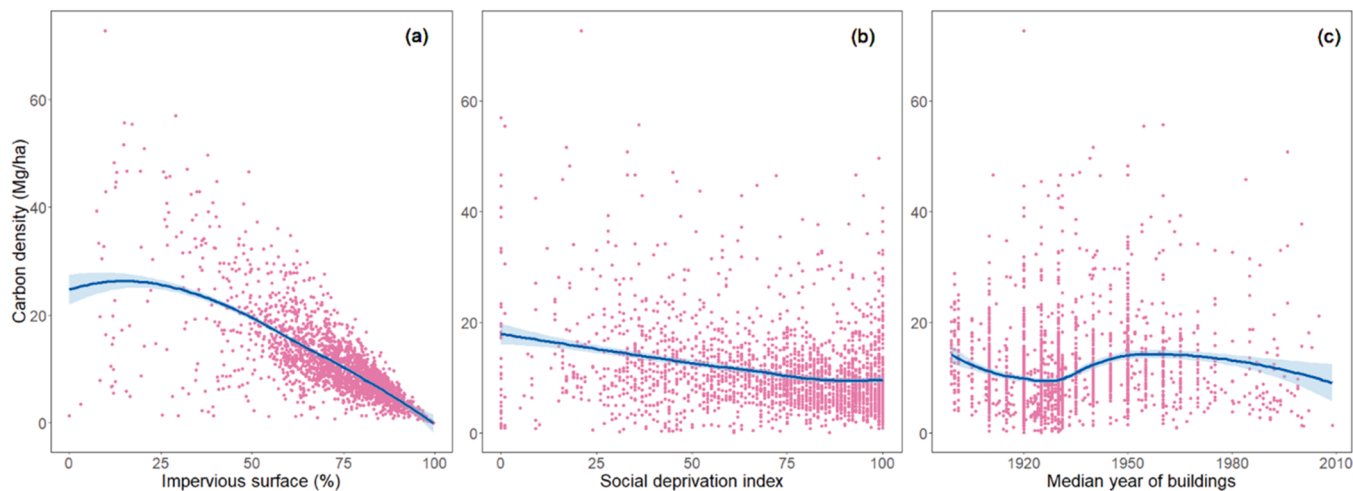


Fig. 7. Variations of carbon density in urban trees across (a) urban development intensity (indicated by percentage of impervious surface); (b) social gradient of deprivation; and (c) neighborhood age (indicated by median age of all constructed buildings on land parcels). The blue smooth curve in the graph represents a general pattern between the explanatory and dependent variables, which was produced by the LOESS nonparametric regression fitting with the .75 for span and 2 for degree of the polynomials.

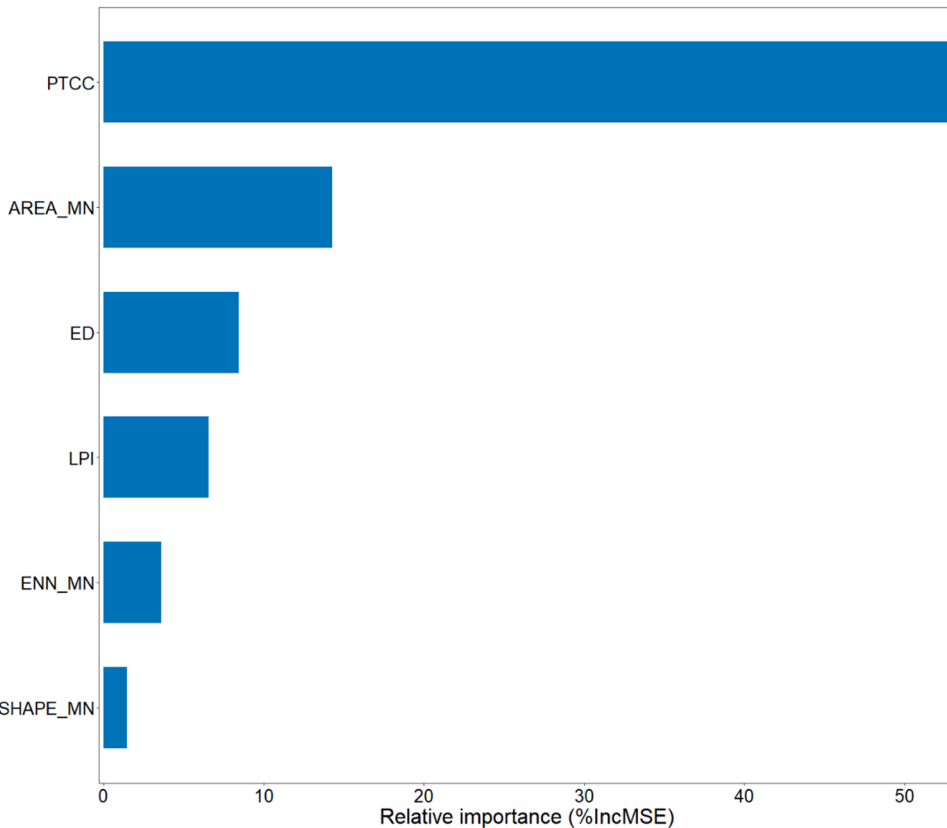


Fig. 8. Relative importance of landscape metrics in explaining carbon densities.

urban parks and residential land, while lowest in commercial and industrial lands. Street trees have the second largest carbon density (12.2 Mg/ha) among all land uses, which is unexpected given stressful roadside environments (e.g., high vehicle pollutant emissions, and physical damages introduced by vehicles and vandals). A slightly higher value (13.9 Mg/ha) is reported in street trees in Beijing, and the authors explain that it is probably because higher temperatures and rising levels of carbon concentration and nitrogen deposition from for example roadside emissions enhanced tree growth (Tang et al., 2016). In

addition, a variety of tree management and stewardship activities in NYC may be more beneficial to street trees than the others due to the accessibility of street trees (Campbell et al., 2014).

Carbon density declines greatly with increased impervious surfaces. This pattern is well observed in other studies that examined the relationship between urbanization and carbon outcomes (Godwin et al., 2015; Hutyra et al., 2011; Sun et al., 2019). It might be attributed to competing for land uses between greenspace and urban development, and increased land development intensities and human disturbances.

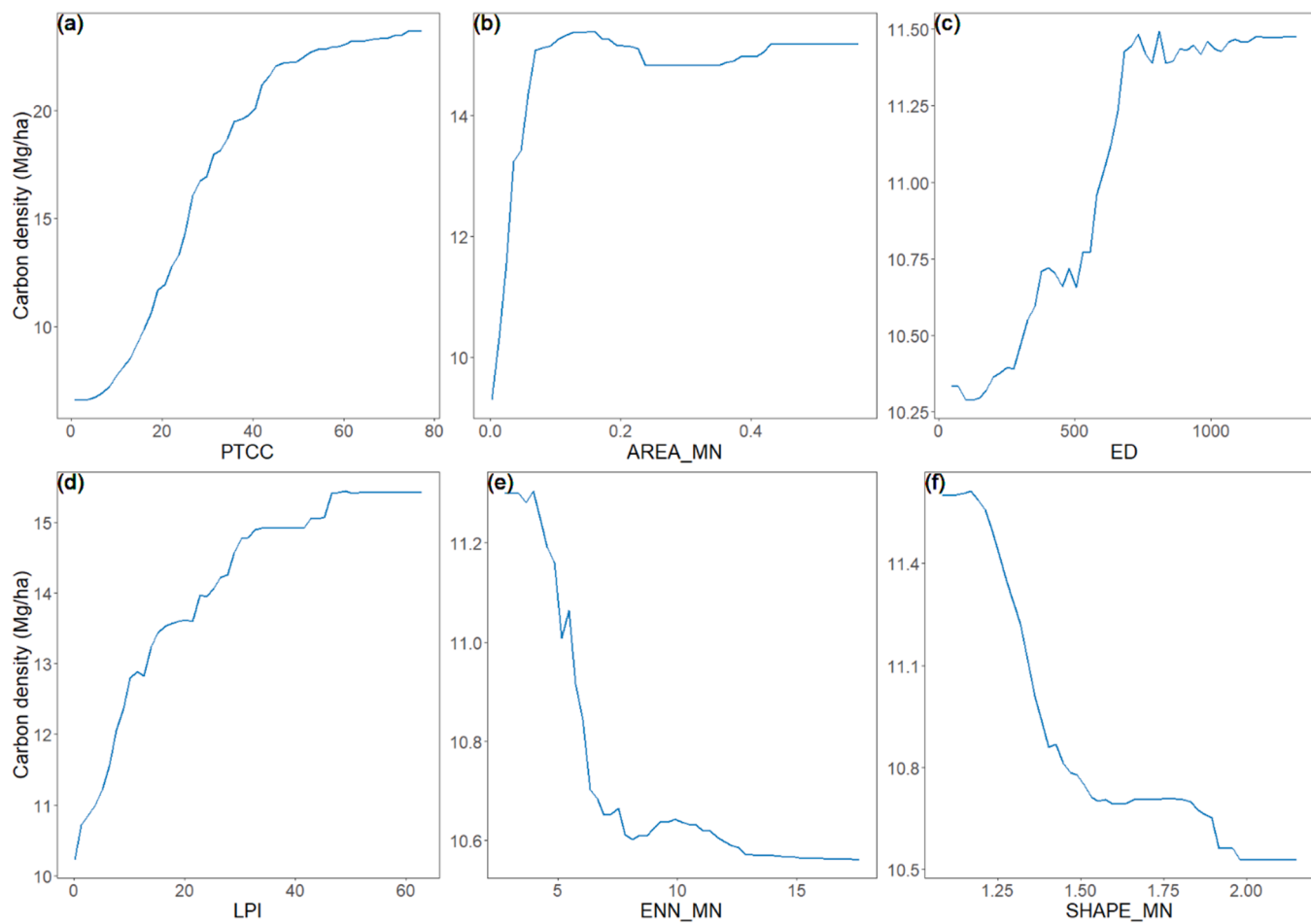


Fig. 9. Partial dependence plots between landscape metrics and carbon density derived from the random forest regression model.

Ren et al. (2011) also explain that higher carbon densities in less urbanized areas is attributed to the implementation of reforestation programs in the suburban and exurban areas. This indicates that tree planting and management could potentially ameliorate the negative impacts of urbanization. Regarding the relationship between tree carbon and urban residents, it varies depending on specific socioeconomic and demographic characteristics considered (Raciti et al., 2014). By employing the SDI that reflects the differences in income, education, employment, living status, housing quality, and transportation, we reveal that socially vulnerable groups (indicated by high SDI scores) are associated with lower carbon densities. This raises environmental justice concerns. It has been well-recognized that socially vulnerable and economically disadvantaged groups are typically less prepared and disproportionately exposed to and affected by climate hazards (Hobbie and Grimm, 2020). In line with existing literature, our finding confirms the environmental justice issue regarding carbon density, which represents a lost opportunity and a future potential to sequester carbon in communities where climate change mitigation efforts are needed the most.

For neighborhood age and carbon density, there existed a complicated relationship, with the minimal and peak carbon densities identified in neighborhoods built in 1920 s and 1950 s, respectively. Neighborhood age is one of the most influential built factors to explain tree abundance, and the neighborhood age and its higher-order terms are commonly employed to predict tree cover variability (McPherson et al., 2013; Pham et al., 2017). This is probably because neighborhood age could reflect the lifecycle of trees and the temporal changes of planning practices (Pham et al., 2017). Conway and Urbani (2007) suggest that urban forest policies should allow for some flexibility to

consider the community age (e.g., replacing dead trees and planting new trees according to the natural lifecycle of trees) so that tree abundance and biomass will not drop off after the peak.

4.3. Comparing carbon densities across cities

We also compiled carbon density estimates of urban forestry from the literature, and conducted an inter-city comparison (Fig. 10). For our focused area (New York City), we found that its carbon density is above the average level, while among the lowest range when compared with other North American cities. When examining other cities, several patterns are learned. First, forests in North American cities have the highest capacity to store carbon (expressed as carbon densities per land area and per tree cover), followed by European cities, while Asian cities' forests have the least capacity. Second, there is a large variability of carbon densities across cities, especially for North American cities. Third, the relationships between carbon densities and city sizes are not clear, as high carbon densities can be observed in both small and large cities.

The comparison of findings across cities is meaningful and could have some practical implications. While cities are in different climatic zones and in different development stages i.e., Asian cities may be in a rapid process of urbanization while North American cities may be in a more mature and conservation stage, there are definitely some lessons and management experiences that could be summarized from the cities in the top-right of Fig. 10. For example, many urban forest programs in North American cities are good at rallying stakeholders from diverse backgrounds and forming collaborations and partnerships across public institutes, private sectors, non-profit organizations, community partners and citizen volunteers (Campbell et al., 2014). This has important

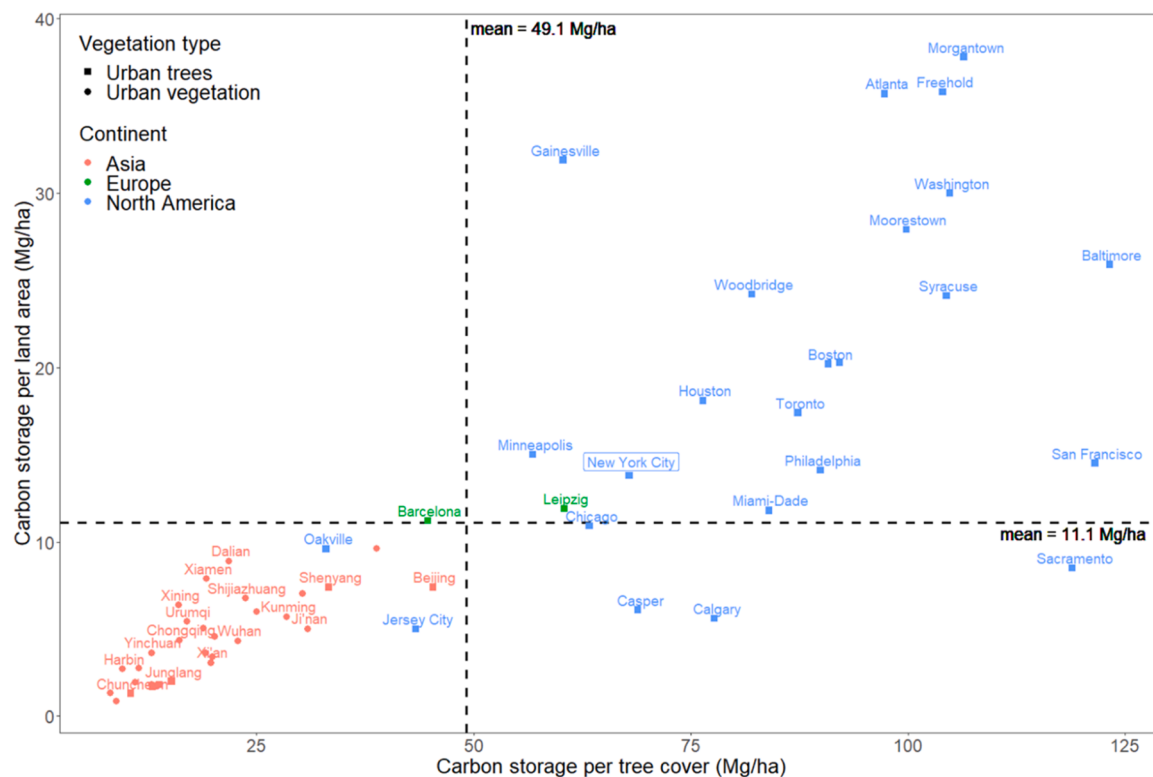


Fig. 10. A comparison of carbon storage normalized by land area and tree cover across a range of cities compiled from the literature. Urban vegetation means a combination of trees, shrubs and grass. If the carbon storage per land area is not provided by the papers, we calculated it by dividing the carbon storage total by the urban built-up area.

implications for cities that are facing a shortage of staff and funding and do not have dedicated local governments.

4.4. Relationships between tree morphology and carbon density

Urbanization and urban development dramatically modify the landscape structure. However, the impacts of this modification on carbon density and natural climate adaptation remain largely unexplored. While increasing the percentage of canopy cover (PTCC) has the strongest positive effect on carbon density, the opportunity will eventually become saturated due to competing land uses and limited land resources in urban areas. Our results show that specific aspects of greenspace design could potentially complement this limitation by storing additional carbon. We find that maintaining the mean area of tree cover (AREA_MN) is more important than the largest tree cover patch (LPI), in terms of adding carbon densities. The association between AREA_MN and carbon density levels off when TCC is larger than 0.1 ha. This indicates that small-sized TCCs (e.g., small green land parcels, pocket parks, and neighborhood parks) are important and sufficient to support the carbon benefits of trees.

Similar level-off patterns are also observed for LPI and ED, which indicates that small- and medium-sized forests and moderate levels of edges are also beneficial for carbon storage. This finding suggests that urban forests behave differently from traditional forest ecosystems, which favor the belief that forest sizes must be large enough and fragmentation must be minimized to maintain high forest interior to edge ratios (Brinck et al., 2017). Two recent studies in the Northeast US also find the enhanced growth of trees around the edges of urban forests, and small forest patches play an outsized role in combatting climate change (Garvey et al., 2022; Morreale et al., 2021). In urban ecosystems, when fragmentation and more edges are unavoidable and become a new normal, it is important to take them into account for developing innovative solutions and landscape designs. Our findings also suggest that

increased aggregated pattern of TCC (ENN_MN) and compact shape of TCC (SHAPE_MN) are associated with higher carbon densities. However, their impacts are much smaller than other landscape metrics.

4.5. Limitations and future studies

Although our study quantifies and maps carbon storage in urban trees, we do not evaluate the full carbon mitigation potential of urban forestry. Below we outline several important carbon outcomes of urban forestry that are not explicitly considered by our study. First, we do not quantify carbon stored in other important carbon pools (e.g., urban soils, and down woody materials) (Pregitzer et al., 2021). In addition, carbon sequestration and loss due to tree growth, natural mortality and decomposition, and tree management are also ignored here. Second, we do not quantify the indirect effects of urban trees on carbon outcomes. For example, tree-related management activities and machinery operations could lead to carbon emissions while urban trees could provide evaporative cooling and shading effects to reduce energy use of nearby residential buildings (Nowak et al., 2017). Third, we focus on only urban trees while ignoring other vegetation types (e.g., shrubs and grasses) that may also have large carbon mitigation potential.

It is feasible to quantify diverse carbon pools, carbon dynamics, and the indirect carbon outcomes of urban trees by providing additional datasets (e.g., soil sampling and measures, time-series field plot measures, and building energy consumption and location of building referenced to trees). However, quantifying carbon storage in shrubs and grasses is challenging as the past and currently proposed urban field surveys provide limited information about shrubs and grasses. For example, the i-Tree Eco field guide and currently ongoing Urban Forest Inventory & Analysis Program in US focus heavily on tree-related measures with only limited attributes for shrubs and grasses (e.g., percentages of shrub and herbaceous covers, and species and height of shrubs) (i-Tree Eco Field Guide, 2021; Urban FIA, 2015). In addition,

unlike trees that have species-specific allometric equations to quantify their carbon amount, shrub and grass carbon is often estimated using different approaches, such as percentage cover-to-biomass equations and diameter-based regression equations (Chojnacky and Milton, 2008), and the uncertainty of such approaches may be large. To fully account for carbon mitigation potential of urban forestry, it is necessary to collect and record relevant attributes and develop more accurate methods.

5. Conclusions

By integrating remote sensing data, i-Tree Eco, and field survey, we produce a high-resolution carbon density map across New York City (NYC), examine the variability of carbon across multiple dimensions of urban landscapes, and explore relationships between tree morphology and carbon density. We estimate that carbon stored in urban trees is 1078 Gg (13.8 Mg/ha normalized by land area and 67.8 Mg/ha normalized by tree cover) for NYC. This large amount of carbon is unevenly distributed, and carbon densities are high in open space & park and street land, in areas with lower urban development intensity, and in communities with lower socioeconomic vulnerabilities. Regarding the impacts of tree morphology on carbon density, our results show that while the amount of tree cover is the most influential factor in determining carbon density, small-sized forest patches and moderate levels of forest edges are also conducive to increasing the carbon benefits of urban trees.

Our study, as well as previous studies, demonstrates that urban forestry can provide substantial carbon benefits and is a vital component of natural climate solutions. City managers and policy makers should incorporate urban forestry to develop innovative, effective, and equitable climate mitigation strategies. However, this is not an easy task and requires a better understanding, design, and management of urban forestry. In particular, it becomes even more challenging when considering conflicts with grey infrastructure and other land uses, and trade-offs to fulfill other pressing societal goals. A comprehensive analysis, that engages multiple stakeholders and allows for synergies and trade-offs between multiple ecosystem services, is necessary to support strategic decision-making.

CRediT authorship contribution statement

Jian Lin: Conceptualization, Methodology, Software, Data curation, Writing – original draft; **Qin Ma:** Data curation, Software, Validation, Writing – review & editing; **Yang Ju:** Validation, Writing – review & editing; **Hongsheng Zhang:** Visualization, Investigation, Writing – review & editing; **Qiang Wang:** Software, Validation; **Bo Huang:** Supervision.

Declaration of Competing Interest

The authors declare that they have no known competing financial interests or personal relationships that could have appeared to influence the work reported in this paper.

Data Availability

Data will be made available on request.

Acknowledgements

Special thanks to Dr. David Nowak and the USDA Forest Service Northern Research Station for providing the field survey data in New York City.

References

- Alberti, M., 2005. The effects of urban patterns on ecosystem function. *Int. Reg. Sci. Rev.* 28 (2), 168–192.
- Breiman, L., 2001. Random forests. *Mach. Learn.* 45 (1), 5–32.
- Brinck, K., Fischer, R., Groeneweld, J., Lehmann, S., Dantas De Paula, M., Pütz, S., Sexton, J.O., Song, D., Huth, A., 2017. High resolution analysis of tropical forest fragmentation and its impact on the global carbon cycle. *Nat. Commun.* 8 (1), 1–6.
- Butler, D.C., Petterson, S., Phillips, R.L., Bazemore, A.W., 2013. Measures of social deprivation that predict health care access and need within a rational area of primary care service delivery. *Health Serv. Res.* 48 (2pt1), 539–559.
- Campbell, L.K., Monaco, M., Falxa-Raymond, N., Lu, J., Newman, A., Rae, R.A., Svendsen, E.S., 2014. Million TreesNYC: the integration of research and practice. N. Y., NY: N. Y. City Parks Recreat. 1–43, 43.
- Chen, W.Y., 2015. The role of urban green infrastructure in offsetting carbon emissions in 35 major Chinese cities: a nationwide estimate. *Cities* 44, 112–120.
- Chicco, D., Warrens, M.J., Jurman, G., 2021. The coefficient of determination R-squared is more informative than SMAPE, MAE, MAPE, MSE and RMSE in regression analysis evaluation. *PeerJ Comput. Sci.* 7, e623.
- Chojnacky, D.C., Milton, M., 2008. Measuring carbon in shrubs. In: *Field Measurements for Forest Carbon Monitoring*. Springer, pp. 45–72.
- Conway, T.M., Urbani, L., 2007. Variations in municipal urban forestry policies: a case study of Toronto, Canada. *Urban For. Urban Green.* 6 (3), 181–192.
- Davies, Z.G., Dallimer, M., Edmondson, J.L., Leake, J.R., Gaston, K.J., 2013. Identifying potential sources of variability between vegetation carbon storage estimates for urban areas. *Environ. Pollut.* 183, 133–142.
- Fargione, J.E., Bassett, S., Boucher, T., Bridgman, S.D., Conant, R.T., Cook-Patton, S.C., Ellis, P.W., Falcucci, A., Fourqurean, J.W., Gopalakrishna, T., 2018. Natural climate solutions for the United States. *Sci. Adv.* 4 (11), eaat1869.
- Garvey, S.M., Templer, P.H., Pierce, E.A., Reinmann, A.B., Hutyra, L.R., 2022. Diverging patterns at the forest edge: soil respiration dynamics of fragmented forests in urban and rural areas. *Glob. Change Biol.*
- Godwin, C., Chen, G., Singh, K.K., 2015. The impact of urban residential development patterns on forest carbon density: an integration of LiDAR, aerial photography and field mensuration. *Landsl. Urban Plan.* 136, 97–109.
- Grove, J.M., Locke, D.H., O’Neil-Dunne, J.P., 2014. An ecology of prestige in New York City: examining the relationships among population density, socio-economic status, group identity, and residential canopy cover. *Environ. Manag.* 54 (3), 402–419.
- Guan, D., Meng, J., Reiner, D.M., Zhang, N., Shan, Y., Mi, Z., Shao, S., Liu, Z., Zhang, Q., Davis, S.J., 2018. Structural decline in China’s CO₂ emissions through transitions in industry and energy systems. *Nat. Geosci.* 11 (8), 551–555.
- Guo, Q., Li, W., Yu, H., Alvarez, O., 2010. Effects of topographic variability and lidar sampling density on several DEM interpolation methods. *Photogramm. Eng. Remote Sens.* 76 (6), 701–712.
- Hastie, T., Tibshirani, R., Friedman, J.H., Friedman, J.H., 2009. *The elements of statistical learning: data mining, inference, and prediction*. Springer.
- Hobbie, S.E., Grimm, N.B., 2020. Nature-based approaches to managing climate change impacts in cities. *Philos. Trans. R. Soc. B* 375 (1794), 20190124.
- Hutyra, L.R., Yoon, B., Alberti, M., 2011. Terrestrial carbon stocks across a gradient of urbanization: a study of the Seattle, WA region. *Glob. Change Biol.* 17 (2), 783–797.
- i-Tree Eco Field Guide, 2021. i-Tree Eco v6.0 Field Manual. Retrieved from (<http://www.itreetools.org/support/resources-overview/i-tree-manuals-workbooks>). Last accessed Aug, 2022.
- Leff, M. , 2016. The Sustainable Urban Forest: A Step-by-Step Approach, USDA Forest Service USFS Philadelphia Field Station.
- Li, H., Wu, J., 2004. Use and misuse of landscape indices. *Landsl. Ecol.* 19 (4), 389–399.
- Liaw, W., Krist, A.H., Tong, S.T., Sabo, R., Hochheimer, C., Rankin, J., Grolling, D., Grandmont, J., Bazemore, A.W., 2018. Living in “cold spot” communities is associated with poor health and health quality. *J. Am. Board Fam. Med.* 31 (3), 342–350.
- Lin, J., Kroll, C.N., Nowak, D.J., Greenfield, E.J., 2019. A review of urban forest modeling: Implications for management and future research. *Urban For. Urban Green.* 43, 126366.
- Lin, J., Wang, Q., Li, X., 2021. Socioeconomic and spatial inequalities of street tree abundance, species diversity, and size structure in New York City. *Landsl. Urban Plan.* 206, 103992.
- Lu, D., 2006. The potential and challenge of remote sensing-based biomass estimation. *Int. J. Remote Sens.* 27 (7), 1297–1328.
- Ma, Q., Su, Y., Guo, Q., 2017. Comparison of canopy cover estimations from airborne LiDAR, aerial imagery, and satellite imagery. *IEEE J. Sel. Top. Appl. Earth Obs. Remote Sens.* 10 (9), 4225–4236.
- McGarigal, K. , 2002. FRAGSTATS: Spatial Pattern Analysis Program for Categorical Maps. Computer software program produced by the authors at the University of Massachusetts, Amherst, (<http://www.umass.edu/landeco/research/fragstats/fragstats.html>).
- McPherson, E.G., Xiao, Q., Aguarón, E., 2013. A new approach to quantify and map carbon stored, sequestered and emissions avoided by urban forests. *Landsl. Urban Plan.* 120, 70–84.
- Morreale, L.L., Thompson, J.R., Tang, X., Reinmann, A.B., Hutyra, L.R., 2021. Elevated growth and biomass along temperate forest edges. *Nat. Commun.* 12 (1), 1–8.
- Nowak, D.J., 1996. Estimating leaf area and leaf biomass of open-grown deciduous urban trees. *For. Sci.* 42 (4), 504–507.
- Nowak, D.J., Appleton, N., Ellis, A., Greenfield, E., 2017. Residential building energy conservation and avoided power plant emissions by urban and community trees in the United States. *Urban For. Urban Green.* 21, 158–165.

- Nowak, D.J., Crane, D.E., 2002. Carbon storage and sequestration by urban trees in the USA. *Environ. Pollut.* 116 (3), 381–389.
- Nowak, D.J., Crane, D.E., Stevens, J.C., Hoehn, R.E., Walton, J.T., Bond, J., 2008. A ground-based method of assessing urban forest structure and ecosystem services. *Arboriculture & Urban. For.* 34 (6): 347-358. 34 6.
- Nowak, D.J., Greenfield, E.J., Hoehn, R.E., Lapoint, E., 2013. Carbon storage and sequestration by trees in urban and community areas of the United States. *Environ. Pollut.* 178, 229–236.
- NYC MOS , 2021). Pathways to Carbon-Neutral NYC. Retrieved from (<https://www1.nyc.gov/assets/sustainability/downloads/pdf/publications/Carbon-Neutral-NYC.pdf>). Last accessed Jun 2022.
- NYC Tree Facts, 2020). MillionTreesNYC: NYC's Urban Forest. Retrieved from (https://www.milliontreesnyc.org/html/urban_forest/urban_forest_facts.shtml). Last accessed Aug, 2022.
- O'Neil-Dunne, J., MacFaden, S., Royar, A., 2014. A versatile, production-oriented approach to high-resolution tree-canopy mapping in urban and suburban landscapes using GEOBIA and data fusion. *Remote Sens.* 6 (12), 12837–12865.
- Pasher, J., McGovern, M., Khoury, M., Duffe, J., 2014. Assessing carbon storage and sequestration by Canada's urban forests using high resolution earth observation data. *Urban For. Urban Green.* 13 (3), 484–494.
- Pham, T.-T.-H., Apparicio, P., Landry, S., Lewnard, J., 2017. Disentangling the effects of urban form and socio-demographic context on street tree cover: A multi-level analysis from Montréal. *Landscape. Urban Plan.* 157, 422–433.
- Pregitzer, C.C., Hanna, C., Charlop-Powers, S., Bradford, M.A., 2021. Estimating carbon storage in urban forests of New York City. *Urban Ecosyst.* 1–15.
- R Core Team, 2022. R: A language and environment for statistical computing.
- Raciti, S.M., Hutyra, L.R., Newell, J.D., 2014. Mapping carbon storage in urban trees with multi-source remote sensing data: Relationships between biomass, land use, and demographics in Boston neighborhoods. *Sci. Total Environ.* 500, 72–83.
- Ren, Y., Wei, X., Wei, X., Pan, J., Xie, P., Song, X., Peng, D., Zhao, J., 2011. Relationship between vegetation carbon storage and urbanization: a case study of Xiamen, China. *For. Ecol. Manag.* 261 (7), 1214–1223.
- Shen, G., Wang, Z., Liu, C., Han, Y., 2020. Mapping aboveground biomass and carbon in Shanghai's urban forest using Landsat ETM+ and inventory data. *Urban For. Urban Green.* 51, 126655.
- Sun, Y., Xie, S., Zhao, S., 2019. Valuing urban green spaces in mitigating climate change: a city-wide estimate of aboveground carbon stored in urban green spaces of China's Capital. *Glob. Change Biol.* 25 (5), 1717–1732.
- Tang, Y., Chen, A., Zhao, S., 2016. Carbon storage and sequestration of urban street trees in Beijing, China. *Front. Ecol. Evol.* 4, 53.
- Urban FIA , 2015. Urban Forest Inventory and Analysis National Program. Retrieved from (<https://www.fia.fs.fed.us/program-features/urban/>). Last accessed Aug, 2022.